Applied Science and Engineering Progress, Vol. 19, No. 4, 2026, 8195

Research Article

X-Band Metamaterial-Based Resonant Sensor for Food Quality Monitoring

Fahmiruddin Esa* and Nurdiana Anis Ibrahim
Department of Physics and Chemistry, Faculty of Applied Sciences and Technology, Universiti Tun Hussein Onn Malaysia, Pagoh, Malaysia

Huda A Majid
Department of Electrical Engineering Technology, Faculty of Engineering Technology, Universiti Tun Hussein Onn Malaysia, Pagoh, Malaysia

Man Seng Sim and Kok Yeow You
Department of Communication Engineering, Faculty of Electrical Engineering, Universiti Teknologi Malaysia, Skudai, Malaysia

* Corresponding author. E-mail: fahmir@uthm.edu.my DOI: 10.14416/j.asep.2026.06.011
Received: 3 March 2026; Revised: 6 April 2026; Accepted: 27 May 2026; Published online: 30 June 2026

Abstract
This paper presents a highly sensitive metamaterial-based resonant sensor operating at X-band for rapid and non-destructive monitoring of food quality. The sensor incorporates an I-beam and C-shaped resonator configuration, with quality assessment achieved through resonant frequency shift and resonance broadening, reflected in the quality factor (Q-factor). The structure was designed and optimized using Computer Simulation Technology (CST) Microwave Studio Suite and experimentally validated using a network analyzer with an X-band rectangular waveguide. The unloaded X-band waveguide-integrated resonator exhibited a high Q-factor of 36.463, suitable for powder characterization. For semi-liquid and liquid samples, a custom 3D-printed cuvette was introduced to improve handling and measurement stability, increasing the Q-factor to 43.498 due to higher moisture sensitivity. The sensor's applicability was demonstrated on cooking powder, oil, and honey. It successfully differentiated soup powder and curry powder with a minimal moisture difference of 0.3%, where increasing moisture content reduced the Q-factor due to enhanced microwave absorption. For honey samples, the Q-factor showed strong correlation with sugar concentration, decreasing with higher glucose and fructose content as reduced free water and increased density altered dielectric properties. Viscosity trends reflect not only sugar concentration but also the influence of bioactive compounds such as polyphenols and flavonoids. In cooking oil analysis, the sensor clearly distinguished fresh and used oil through slight resonant frequency shifts and Q-factor variations, even when FTIR spectroscopy showed limited quantifiable color-related changes caused by oxidation and triglyceride polymerization. Rheological measurements indicated higher viscosity in fresh oil (2.2–2.7 mPa·s) compared to used oil (1.3–1.5 mPa·s), consistent with thermal degradation effects. Overall, the proposed metamaterial sensor demonstrates enhanced sensitivity, compactness, and versatility, confirming its strong potential for real-time industrial food quality monitoring.

Keywords: Metamaterial-based sensor, Q-factor, food quality, X-Band, resonator

1 Introduction

Food quality control constitutes an important area in food industry, ensuring it is safe, reliable, and meets consumer satisfaction. Traditional techniques such as sensory analysis and chemical analysis can be time-consuming, laborious and might not give a non-destructive analysis of the product properties [1], [2]. This limitation has motivated the development of more sophisticated, non-invasive approaches such as microwave sensing, which is extremely sensitive to moisture content, one of the primary indicators of food stability, texture, and shelf-life [3], [4] This approach operates on the principle of investigating the interaction of the microwave signals and dielectric properties on the food, as illustrated by a time-domain reflectometry (TDR) and dielectric spectroscopy [5]–[7]. More recent developments in microwave sensors

employing metamaterials have increased the sensitivity of the detectors to moisture, detectability, and accuracy [8], [9].

Metamaterials are specially made materials that are engineered to regulate electromagnetic waves and their unique properties enable the detection of any characteristic of food in a very sensitive way without altering or affecting the sample, preserving its integrity. The design of microwave metamaterials is tailored to a certain degree to manipulate the microwave frequencies in a manner that cannot be done by natural materials. Substances of this nature are subject to periodic structures which can interact with microwave radiation to produce effects such as negative refraction, improved transmission, or even cloaking [10], [11]. In the context of food quality inspection, microwave metamaterials affect the dielectric properties of food when exposed to microwave radiation [12]. The microwave metamaterials utilized in food monitoring offer a significant advantage in the sensitivity brought by the customization of the structure of the materials.

Water has a strong interaction with microwave radiation, which allows for the detection of moisture changes using microwave metamaterials. This ability is especially valuable in industries like food processing, where precise moisture control is essential, such as in baking, meat processing, and snack production. These sensors can distinguish between foods with different moisture levels by analyzing the shifts in the dielectric constant caused by moisture. As the dielectric properties of food change, the resonator's frequency response also shifts, enabling accurate measurement of moisture and fat content [12]. Microwave metamaterials can also evaluate the fat and protein content in food, as these substances affect its dielectric properties. By customizing the metamaterial sensor to respond to specific frequencies, a system can be designed to selectively detect changes in fat and protein levels.

Recent studies have shown the potential of microwave metamaterials in analyzing dairy products and meats, offering precise fat content measurements without the need for chemical additives [13], [14]. Furthermore, microwave metamaterial sensors can identify contaminants such as foreign objects (metal or plastic) within food products. When microwaves interact with different materials, their reflection or absorption characteristics change. By leveraging metamaterials, sensors can become highly sensitive to these changes, enabling early detection of contaminants that could pose safety risks to consumers. Another significant advantage of microwave metamaterial sensors is their ability to non-destructively inspect the internal structure of food products. For example, microwave metamaterials can assess the uniformity of food processing (such as cooking or freezing) and detect defects like air pockets, ice crystallization, or uneven cooking in products like frozen vegetables or meat [15]–[17]. This capability ensures that food products maintain their desired texture and appearance.

Despite these developments, most metamaterial-based microwave sensors reported in the literature are based on planar or multi-unit resonator designs and are primarily focused on biomedical or material analysis applications, with less emphasis on food quality sensing in a controlled waveguide setup. The use of compact single-unit metamaterial resonators in rectangular waveguide systems for food sensing, especially in the X-band frequency range, which is highly sensitive to dielectric changes, has been less explored. Most food products have high moisture content, which can make it difficult for a resonator sensor to detect frequency shifts unless the sensor has a high-quality factor (Q-factor). Therefore, it is important to use a resonator with a high Q-factor, as this indicates a sharper and more well-defined resonance dip [18], [19]. Integrating the resonator with an X-band waveguide improves the measurement process by enabling the sample under test to be analyzed in a controlled and convenient manner, while also requiring only a small sample volume due to its compact size. This configuration avoids inaccuracies and increases stability by operating as a closed measurement system, where microwave radiation is confined and prevented from propagating into unwanted or external media [20]–[22].

To address the research gap, this research aims to provide a compact metamaterial-based resonant sensor using a hybrid I-shaped and C-shaped resonator in an X-band rectangular waveguide. The sensor is designed and simulated using CST Studio Suite to improve the localization of the electromagnetic fields while ensuring simplicity and stability in the structure. The sensor is fabricated and measured using food samples in both powder and liquid forms, and the sensing capability of the sensor is evaluated based on the analysis of the shifts in the resonant frequency corresponding to the variations in the moisture content, sugar concentration and material composition of the food samples.

2 Materials and Methods

2.1 *Design and simulation of a metamaterial-based sensor*

The design of the metamaterial-based sensor was inspired by [23], with specific dimensions shown in Figure 1 (a); however, this work utilizes only a single-cell metamaterial, which was selected to simplify fabrication while maintaining strong electromagnetic field localization and higher resonance sensitivity. The design is essentially a combination of I-beam and C-shaped structures, with a mirrored replication to form a pair of designs. This hybrid geometry was intentionally selected to exploit the strong current distribution of the I-beam and the capacitive gap effects of the C-shaped resonator, which improve field confinement and high-quality factor (Q-factor).

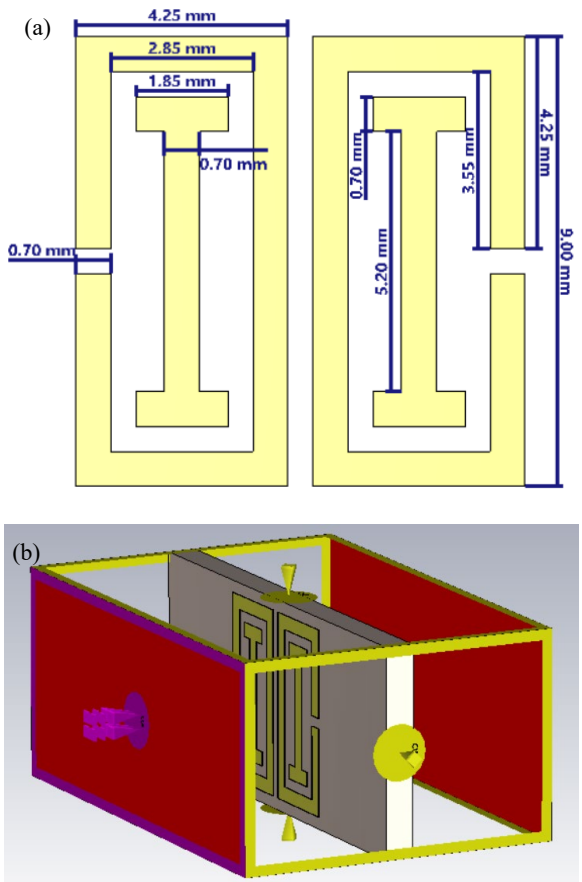

Figure 1: (a) Dimension of the copper structure (b) defined boundary conditions for the simulation model.

The sensor was created using CST Microwave Studio Suite software. It features a copper structure mounted on a 1.4 mm FR-4 substrate, with a thickness of 35 µm. FR-4 was selected due to its mechanical stability, cost-effectiveness, and suitability for X-band microwave applications. The overall substrate size conforms to the American Electronic Industries Alliance (EIA) Standards for WR90 X-band rectangular waveguide dimensions.

The boundary conditions for the designed sensor are illustrated in Figure 1 (b), where the top, bottom, and side walls are defined as conducting walls, while the front and back are modeled as open space. This configuration provides a controlled environment for waveguiding and improves resonance stability, enabling precise interaction between the electromagnetic fields and the sensor structure. This open area is the transmission medium of the waves, and the simulation method used in this case is a reflection and transmission method. However, the properties of reflection are only considered relevant in the application of sensing detection. The metamaterial-based sensor successfully demonstrated a resonant frequency of approximately 10.7 GHz. This resonance is known for its sharpness and localization at the resonator's edges and gaps, making it sensitive to even minor dielectric changes caused by food materials.

2.2 *Fabrication and measurement of a metamaterial-based sensor*

The designed sensor was outsourced to JAC Engineering Sdn Bhd for high-precision fabrication due to its small size. After fabrication, the sensor was precisely inserted into the rectangular waveguide, as shown in Figures 2 (a) and (b). It was then connected to an X-band waveguide adapter and an N5234B PNA-L Microwave Network Analyzer to complete the detection system. This detection technique is suitable for various types of samples, including solids, semi-solids like paste, powders, and liquids. The volume required for both solid and pressed powder samples matches that of the X-band rectangular waveguide cavity used in this study, which measures 22.86 × 10.16 × 3 mm. The powder sample was manually compacted using a specialized pelletizing tool with the same dimensions as the rectangular waveguide and pressed by hand to ensure conformity with the cavity's shape.

For liquid samples, a holder (customized cuvette) made from a low-loss material must be used

Applied Science and Engineering Progress, Vol. 19, No. 4, 2026, 8195

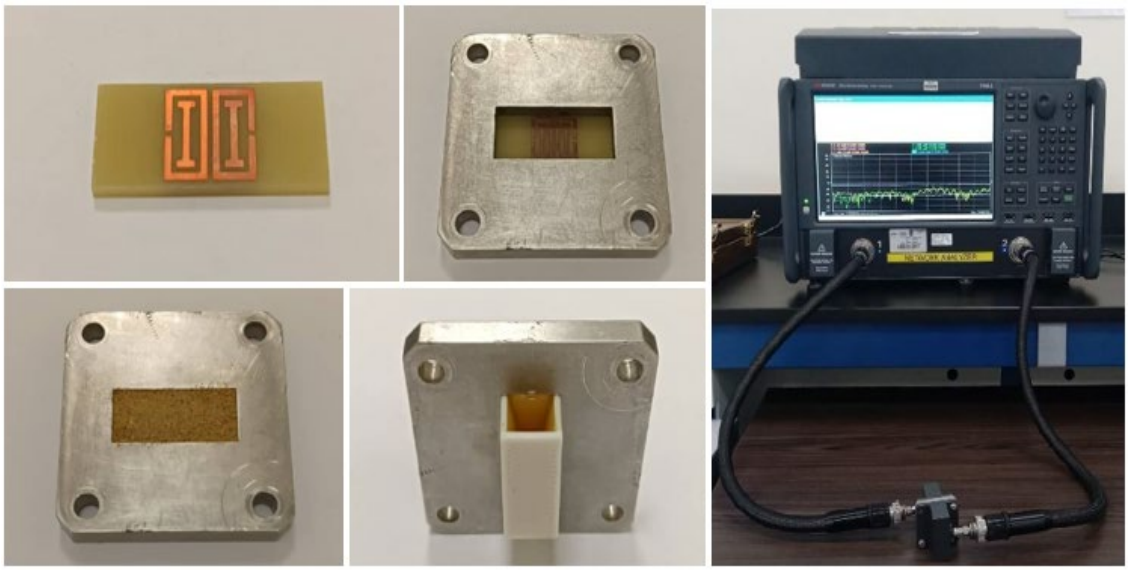

Figure 2: (a) Fabricated metamaterial-based sensor (b) metamaterial-based sensor fit into the X-band rectangular waveguide holder (c) powder sample configuration (d) liquid sample configuration (e) measurement setup.

to prevent significant signal loss. The cuvette was designed using CST Microwave Studio Suite and fabricated using a 3D printing technique with Polyethylene Terephthalate Glycol (PETG) filament. PETG is a thermoplastic polyester known for its durability, chemical resistance, and ease of processing. It also exhibits favorable dielectric properties, making it suitable for use in radio frequency (RF) and microwave applications. Additionally, PETG exhibits high volume resistivity, indicating excellent insulating properties.

The outer dimensions of the cuvette were designed to match the size of the rectangular waveguide, allowing it to fit securely within the cavity. With a wall thickness of 1 mm, the resulting inner dimensions of the cuvette are 21.86 × 8.16 mm, and with a length of 10 mm, the internal volume is approximately 1,784 mm³. The cuvette is open at the top, with only the bottom part serving as the base. Figure 2 (d) illustrates a perspective view of the cuvette integrated with the metamaterial-based sensor in the rectangular wave cavity. Figures 2(c) and 2(d) illustrate the sample setup configurations for the powder and liquid samples under test, respectively, while Figure 2(e) presents the complete measurement setup. Transmission-reflection-line (TRL) calibration was performed in the X-band frequency range to provide accurate reference planes for the waveguide ports, ensuring the accuracy of the sensing measurement.

2.3 *Material Characterizations*

2.3.1 *Moisture content*

Three types of commercial cooking powders were tested: turmeric powder (TuP), soup powder (SoP), and curry powder (CuP). These samples have been selected based on their ability to represent different powdered food products that are commonly consumed and have different compositions, processing methods, and moisture retention characteristics, thus making them useful for assessing the sensor's sensitivity to small moisture variations. Moisture content (MC) of these powders was determined by using A&D Weighing MX-50 Moisture Analyzer, 0.001g of accuracy, with a 5g initial weight of sample. Three honey samples: bitter gourd, stingless bee, and nectar were analyzed concurrently. These samples were selected based on their distinct botanical origins, which are likely associated with variations in moisture and sugar content. Such differences provide an appropriate range for evaluating the sensor's response to liquid food samples. These honey samples were dried in a conventional oven (Memmert UF110). Triplicate weighing gave almost the same final dried mass for every sample, illustrating consistency and reproducibility between replicates as shown in Tables 1 and 2. The average value of these measurements was then used to determine the moisture content percentage using equation (1),

$$MC = \frac{Initial\ mass - Dried\ mass}{Initial\ mass} \times 100\% \quad (1)$$

Table 1: Moisture content (%) of different types of cooking powders.

Sample	Dried sample mass (g)			Average mass (g)	Moisture content (%)
	1st	2nd	3rd		
CuP	4.553	4.545	4.567	4.555	8.900
SoP	4.534	4.544	4.541	4.540	9.200
TuP	4.401	4.391	4.390	4.394	12.120

Table 2: Moisture content (%) of different types of honey.

Sample	Trial	Petri dish (g)	Wet sample (g)	Petri dish + dried sample (g)	Moisture content (%)
Nectar honey	1st	17.4642	0.5162	17.8757	20.28
	2nd	17.6586	0.5139	18.0679	20.35
	3rd	17.8075	0.5142	18.2169	19.88
Mean		17.6434	0.5147	18.0535	**20.17**
Bitter gourd honey	1st	17.6377	0.5121	18.0364	22.14
	2nd	17.6789	0.5135	18.0784	22.20
	3rd	17.8234	0.5134	18.2245	21.87
Mean		17.7133	0.5130	18.1131	**22.07**
Stingless bee honey	1st	17.8128	0.5134	18.1779	28.88
	2nd	17.4277	0.5122	17.7924	28.80
	3rd	17.5046	0.5141	17.8704	28.85
Mean		17.5817	0.5132	17.9469	**28.84**

2.3.2 *Sugar content*

The sugar content of the honey samples was determined using a digital handheld refractometer (ATAGO PAL), with the final value calculated as the average of three independent readings, as presented in Table 3.

Table 3: Sugar content (Brix %) of different types of honey.

Sample	Trial			Brix %
	1st	2nd	3rd	
Nectar honey	80.30	80.30	80.40	80.33
Bitter gourd honey	78.50	78.60	78.60	78.57
Stingless bee honey	72.80	73.00	73.00	72.93

2.3.3 *FTIR spectroscopy*

Fourier Transform Infrared Spectroscopy (FT-IR) was performed with a Spectrum Two™ FT-IR spectrometer (PerkinElmer) to analyze cooking oil and honey samples. Measurements were performed in the mid-infrared region by choosing a spectral range from 4000cm^{-1} to 400 cm^{-1} with 1 cm^{-1} resolution. Ten scans were acquired for each sample to attain a suitable signal-to-noise ratio. Spectra were recorded and collected using the Spectrum software. FTIR does not provide any direct quantitative relationship with electromagnetic parameters, but the detected chemical functionalities offer supporting insight into the change in moisture content, sugar composition, and oxidation products that contribute to the dynamics of dielectric properties after the response of a microwave sensor.

2.3.4. *Viscosity*

Rheological measurements of cooking oil (palm oil type) and honey were performed using a Hybrid Rheometer HR20 (TA Instruments) to evaluate the flow behavior of the samples. The analysis was conducted under controlled conditions at a fixed room temperature of 25 °C. A viscosity versus shear rate test was carried out to assess the characteristics of the materials. Shear rate was systematically varied, and the corresponding viscosity values were recorded using the rheometer's integrated software. This method enables the characterization of the flow properties and viscosity profiles of the samples under varying shear conditions.

3 Results and Discussion

3.1 *Metamaterial-based sensor characteristics*

Figure 3 presents the reflection coefficient of the proposed metamaterial-based sensor in the X-band frequency range. The measured resonant frequency (f_o) is observed at 10.720 GHz, where the reflection coefficient reaches a minimum value of 0.453. This resonant behavior is consistent with the simulation result obtained using CST Microwave Studio. The bandwidth (bw_o) at full width half maximum (FWHM) is 0.294 GHz, corresponding to a reflection coefficient of approximately 0.7, with the minimum and maximum frequencies at 10.594 GHz and 10.888 GHz, respectively. The quality factor, Q-factor (Q_o) quantifies the sensor sensitivity, which is related to resonant frequency and bandwidth by the formula, $Q_o = \frac{f_o}{bw_o}$. According to the formula, this resonator has a narrow and a high Q-factor of 36.463.

Figures 4 and 5 show contour plots representing the electric and magnetic field distributions, respectively, of the copper-structured metamaterial on an FR-4 substrate at three different frequencies: 10.5 GHz, 10.7 GHz, and 11.0 GHz. The red contours denote regions of maximum electric and magnetic field intensities, whereas the blue contours indicate

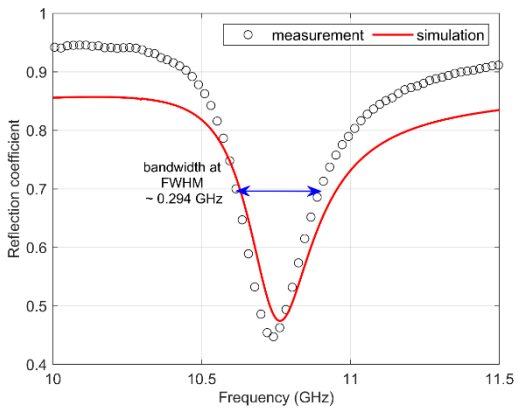

Figure 3: Reflection coefficient against frequency of the metamaterial-based sensor

regions of minimum field intensities. The maximum electric field achieves 40 dB(V/mm) near the resonance frequency at 10.7 GHz. The electric field distribution is primarily concentrated around the top and bottom edges of the I-beam and the split gap structure of the C-shaped copper structures. In comparison to the other two frequencies, 10.5 GHz and 11.0 GHz, the electric field distribution is mainly driven by the I-beam at 10.5 GHz and by the C-shape at 11.0 GHz, respectively. The magnetic field, dB(A/mm), distribution follows a similar trend but with different orientations. For instance, the electric field is more concentrated at the flange side of the I-beam, while the magnetic field is concentrated at the web side. Conversely, at the C-shaped structure, the electric field is more concentrated at the notch areas, while the magnetic field is focused at the inside of the right angle (90°). Moreover, the concentration of the electric field between the gaps of the structure enables better coupling with the material under test, which is vital for detecting small variations in the dielectric constant. All these features ensure that the configuration consisting of the I-beam and C-shaped structure offers better electromagnetic confinement.

3.2 *Metamaterial-based sensor loaded with compacted cooking powder*

Figure 6 displays the reflection coefficient characteristics for three different types of commercial cooking powders tested using the metamaterial-based sensor.

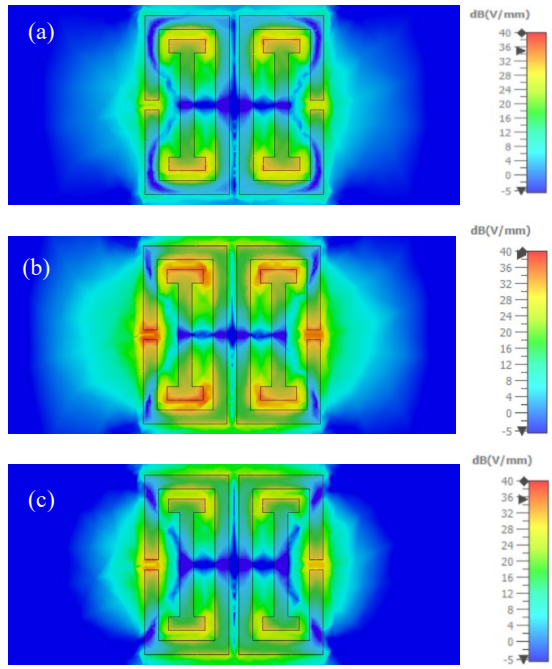

Figure 4: Electric field distribution of metamaterial-based sensor at (a) 10.5 GHz (b) 10.7 GHz and (c) 11.0 GHz.

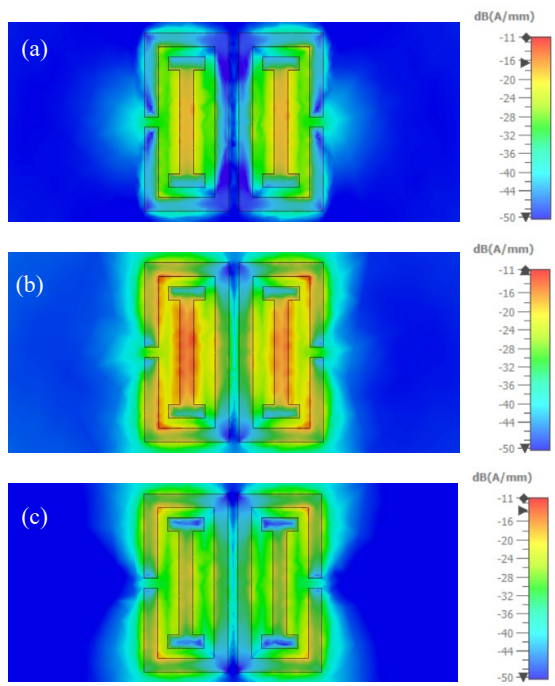

Figure 5: Magnetic field distribution of metamaterial-based sensor at (a) 10.5 GHz (b) 10.7 GHz and (c) 11.0 GHz.

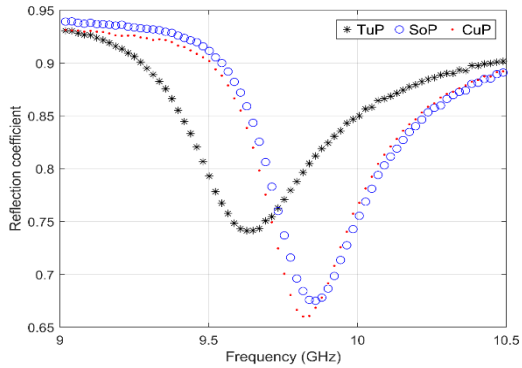

Figure 6: Reflection coefficient against frequency of the metamaterial-based sensor loaded with various cooking powders.

The result for TuP shows a significant difference compared to SoP and CuP, which exhibit nearly identical characteristics. Despite this, all results demonstrate distinct features, with only a slight variation between SoP and CuP, which is 0.3 % difference. This indicates that the metamaterial-based sensor is highly sensitive, owing to the intrinsic permittivity properties of each powder type. The differences in permittivity are likely due to variations in the materials' composition and moisture content [24], [25]. Among these factors, moisture content plays a critical role in the quality and shelf life of food products like powders [1,3]. As the moisture content increases, a corresponding reduction in Q-factor and an increase in bandwidth are consistently observed, as presented in Table 4. This is due to increased microwave absorption because of increased losses associated with the presence of water molecules.

Table 4: Sensing characteristics and moisture content of tested cooking powders.

Parameters	Turmeric Powder (TuP)	Soup Powder (SoP)	Curry Powder (CuP)
Resonant frequency (f_s), GHz	9.628	9.859	9.817
Reflection coefficient	0.741	0.675	0.660
FWHM	0.839	0.806	0.797
Bandwidth (bw_s), GHz	0.504	0.399	0.378
Quality factor (Q_s)	19.103	24.709	25.971
Moisture content (%)	12.120	9.200	8.900

Repeated measurements showed stable resonant frequencies with negligible variation, indicating good repeatability of the sensing response, although minor uncertainties may arise from manual powder compaction and sample packing density. Overall, the proposed metamaterial-based sensor is very sensitive to even the slightest changes in the dielectric properties of the powdered food product and is therefore suitable for nondestructive sensing and quality control.

3.3 *Metamaterial-based sensor loaded with semi-liquid samples (honey)*

Figure 7 shows the reflection coefficient characteristics for different types of honey. The fundamental characteristics of the unloaded liquid samples differ due to the presence of the cuvette, which was considered in the total reflection coefficient as a reference. The resonant frequency for the reference shifted to a lower value of 10.048 GHz, representing a reduction of approximately 0.7 GHz from the previous measurement without the cuvette, while the minimum reflection coefficient remained nearly the same. The Q-factor increased to 43.498, with the bandwidth at FWHM measured at 0.231 GHz. The observed increase in Q-factor under the unloaded condition with the PETG cuvette is attributed to its function as a low-loss dielectric interface, which mitigates radiation and impedance mismatch losses while enhancing electromagnetic field confinement around the resonator. Consequently, energy storage is improved and the resonance becomes sharper compared to the configuration without the PETG cuvette, consistent with predictions from cavity perturbation theory [26], [27].

Loading honey into the cuvette successfully activated the sensing mechanism, leading to a noticeable frequency shift and broader resonance peaks. The reflection coefficient increased, indicating a lower Q-factor compared to the cooking powder samples. This behavior is attributed to greater energy absorption resulting from the higher moisture content of the honey samples. [28-30]. Nectar honey has a relatively smaller resonant frequency shift with a higher Q-factor, which can be explained by the high concentration of glucose-fructose and low free water content [31].

Table 5 indicates that the nectar honey contained the highest average sugar content of 80.33%, the stingless bee honey contained the lowest sugar level

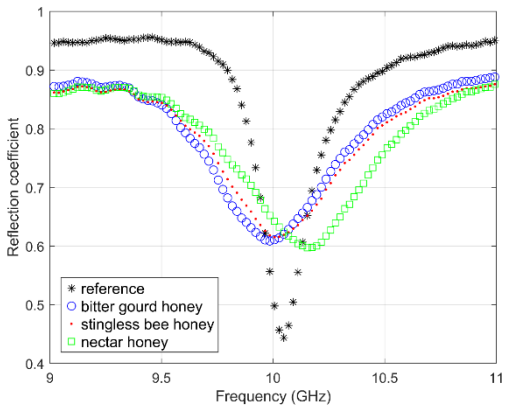

Figure 7: Reflection coefficient against frequency of the metamaterial-based sensor loaded by different types of honey.

with 72.93% and the bitter gourd honey had an intermediate range with an average sugar content of 78.57%. The sugars that were predominant were glucose and fructose, which are the main carbohydrates in honey and strongly influenced its physical properties, such as the viscosity and moisture content [32]. The increased concentration of glucose and fructose in nectar honey causes high density and a reduced amount of free water. This treatment results in a separation of microwave absorption properties. Inversely, stingless bee honey has lower sugar content but higher moisture [33]. These compositional variations affect shelf life, crystallization and sensory characteristics, as will be elaborated in the FTIR and viscosity analysis (Figure 8 and Figure 9). These alterations directly affect rheological behavior and the existence of functional groups attached to sugars and polyphenolic compounds.

Table 5: Sensing characteristics, moisture and sugar content of diffèrent types of honey.

Parameters	Stingless Bee Honey	Bitter Gourd Honey	Nectar Honey
Resonant frequency (f_s), GHz	10.006	9.985	10.153
Reflection coefficient	0.615	0.609	0.597
FWHM	0.748	0.749	0.742
Bandwidth (bw_s), GHz	0.588	0.588	0.672
Quality factor (Q_s)	17.017	16.981	15.109
Moisture content (%)	28.84	22.07	20.17
Sugar content (Brix %)	72.93	78.57	80.33

The FTIR spectroscopy analysis of nectar, bitter gourd honey, and stingless bee honey displays the functional group compositions and molecular structures among the samples. As shown in Figure 8, the broad absorption band centered at 3271 cm^{-1} is attributed to O–H stretching vibrations, indicating that honey contains the hydroxyl groups that are typical of sugars and phenolic substances. The wide peak indicates that all the honey samples had a significant amount of moisture, which is important for the texture as well as the preservation of honey. The peaks at 2927 cm^{-1} refer to the aliphatic hydrocarbons, which are present in the sugar portions of honey, corresponding to the C-H stretching vibrations. The peak at 1643 cm^{-1} is the existence of carbonyl groups, which can be related to aldehyde in glucose and ketones in fructose. The peaks at 1416 cm^{-1} reflected C-H bending vibrations. These bending modes stand for CH_2 and CH_3 groups, demonstrating that honey contains aliphatic structures. The peaks at 1344 cm^{-1} indicate the presence of ether or alcohol [34], [35].

The presence of C-O stretching at peak 1027 cm^{-1} showed a composition of sugar-related chemicals in all honey samples. Peaks at 775 cm^{-1} indicate C-H wagging vibrations. In the fingerprint region (1549–515 cm^{-1}), multiple peaks occur due to C–O, C–C, and C–O–H bending vibrations characteristic of polysaccharides, flavonoids, and phenolic compounds [35]. The FTIR spectra indicate that both botanical source and bee species have a considerable impact on the chemical composition of honey. The carbohydrate-based spectra in nectar honey are typical characteristics of fructose and glucose-rich honey [36]. Bitter gourd honey has spectral characteristics of other organic acids and phenolic compounds. The stingless bees' honey shows a unique spectrum with higher absorbance of both the OH and fingerprint region, which shows a richer polyphenolic content and higher moisture content (Table 5).

The rheological behavior of three samples of honey was assessed to understand the flow behavior of honey. Figure 9 represents viscosity versus shear rate. Nectar honey and stingless bee honey show almost a constant viscosity (0.48–0.49 Pa·s), indicating Newtonian behaviour. This uniformity has been attributed to their water-to-sugar ratios, which maintain structural stability under shear rate [30]. Comparatively, bitter gourd honey exhibits slow

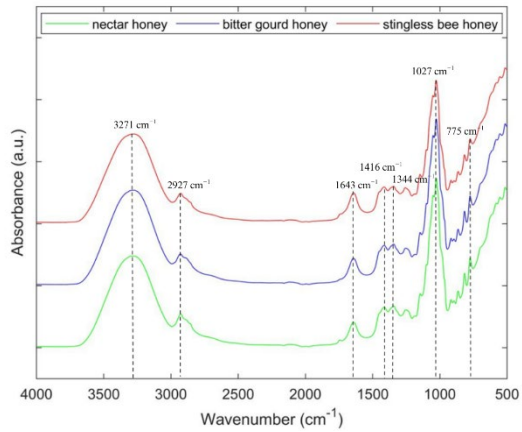

Figure 8: FTIR spectroscopy of different types of honey.

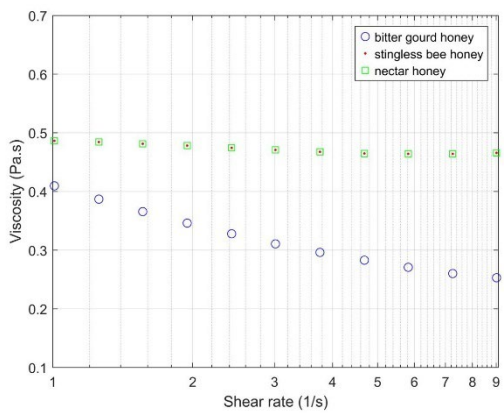

Figure 9: Viscosity as a function of shear rate for different types of honey.

viscosity reduction (0.25-0.40 Pa·s), which is a characteristic of shear-thinning (pseudoplastic) fluids.

The viscosity of nectar and stingless bee honey is higher, which can be attributed to their difference in composition. Honey with a prevalence of nectar and glucose and fructose has a more compact sugar structure and stingless bee honey, though containing less sugar, still has more water and polyphenolics. This increases the intermolecular hydrogen bonding as well as contributes to its viscous behavior [33].

In contrast, bitter gourd honey contains a little less sugar than nectar honey (Table 5) and higher percentages of organic acids, which lower its viscosity and enhance shear-thinning. These trends of viscosity are supplementary to the FTIR results, displaying stronger O-H and C-O bands in stingless bee honey, indicating the presence of higher levels of moisture and polyphenolic compounds, while the spectra of the nectar honey indicate higher levels of carbohydrate functional groups [35]. The results suggest that viscosity is not only dependent on the concentration of sugar but also on the slight bioactive molecules like polyphenols and flavonoids, which contribute to the microstructure through hydrogen bonds and by molecular compounds [37], [38]. On the other hand, viscosity, sugar composition, and moisture content collectively influence the sensor response, confirming the sensitivity of the proposed sensor.

3.4 *Metamaterial-based sensor loaded with liquid (cooking oil)*

Figure 10 presents the reflection coefficient responses of the metamaterial-based sensor loaded with fresh and used cooking oils. Although both samples exhibit resonance shifts toward lower frequencies due to dielectric loading, a measurable frequency difference of approximately 0.1 GHz is observed between fresh and used oils. This proves the high sensitivity and accuracy of the proposed method in detecting differences between oils with closely similar compositions.

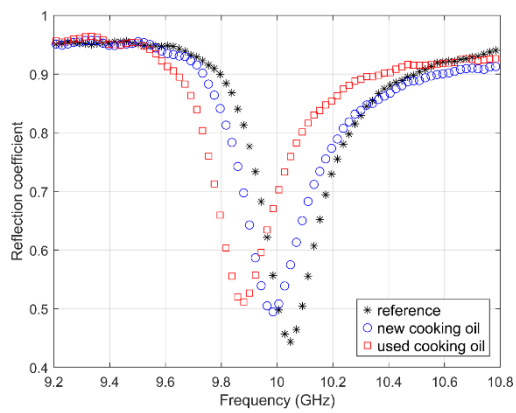

Figure 10: Reflection coefficient against frequency of the metamaterial-based sensor loaded by new and used cooking oil.

As shown in Table 6, the used cooking oil has a lower resonant frequency and a larger reflection coefficient. These observations prove that there are increased losses in the dielectric properties of used cooking oil due to compositional changes. In addition, the used cooking oil has a smaller bandwidth and a larger Q-factor compared to fresh oil. These differences are due to changes in the physical

Applied Science and Engineering Progress, Vol. 19, No. 4, 2026, 8195

Table 6: Sensing characteristics of new and used cooking oil.

Parameters	New Cooking Oil	Used Cooking Oil
Resonant frequency (f_s), GHz	9.985	9.880
Reflection coefficient	0.495	0.512
FWHM	0.726	0.738
Bandwidth (bw_s), GHz	0.294	0.252
Quality factor (Q_s)	33.963	39.206

properties of used cooking oil, particularly a decrease in viscosity due to thermal degradation caused by repeated frying. Triglycerides in the oil are degraded into smaller fragments, which reduces their intermolecular interactions and affects their dielectric properties [39], [40].

Figure 11 shows the FTIR spectra of the new cooking oil and the used cooking oil. The spectra show the chemical characteristics of cooking oil by identifying the functional group peaks and changes in their intensities. The peaks at 2921 cm^{-1} and 2852 cm^{-1} are due to the C–H stretching vibration of the aliphatic –CH2 and –CH3 groups. The existence of the ester carbonyl (C=O) bond due to triglycerides in oil is denoted by the stronger peak at 1743 cm^{-1}. The presence of peaks in the fingerprint area (1500–700 cm^{-1}) indicates various bending and deformation vibrations of hydrocarbon chains and the ester group. The fingerprint region is used to differentiate the identity between the compounds [39], [41]. FTIR bands at 1464 cm^{-1} and 1377 cm^{-1} represent the bending vibration of the alkane group. The peak intensities at 721 cm^{-1} indicate the loss of cis double bonds in cooking oil [42]. The spectra of used cooking oil show changes in intensity and position of some peaks. Notably, there is also an increase in absorbance around 3400 cm^{-1} due to hydroxyl (–OH) functional groups, probably due to byproducts of oxidation. The carbonyl peak of the ester at 1743 cm^{-1} is still present with a new peak at 1600 cm^{-1} and 1100 cm^{-1}, which can be ascribed to carbonyl compounds, as well as oxidation products of aldehydes, ketones, or acids, [39], [42].

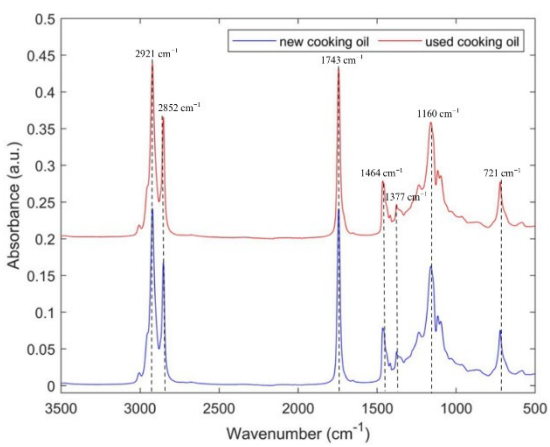

Figure 11: FTIR spectroscopy of new and used cooking oil.

These oxidation-related functional groups increase dielectric loss, thereby enhancing microwave absorption and causing the observed variations in resonant frequency and reflection coefficient. Although FTIR is less sensitive to the early stages of degradation, the joint analysis of electromagnetic and spectroscopic analysis confirms that microwave sensing can detect the subtle variations in composition that are difficult to quantify using FTIR alone.

FTIR spectra of functional groups of new and used cooking oils have numerous similarities, particularly in the presence of characteristic peaks like aliphatic, CH stretching and carbonyl ester. This similarity is expected as the fundamental structure of triglycerides is not usually altered even when they are exposed to heat during frying. However, the baseline absorbance of new and used cooking oil only slightly increases because less unsaturated waste cooking oil is altered [41].

Along with the FTIR result, the used cooking oil showed substantial colour deterioration when compared to the new oil. Along with the FTIR result, the used cooking oil indicated a good colour deterioration compared to the new oil. This visual transformation of light yellow to dark brown is suggested by the oxidation and polymerization of triglycerides that resulted in conjugated carbonyl compounds and polymerized pigments and byproducts of the Maillard reaction [43], [44]. The resulting coloration resulting from oil degradation, reflecting the oxidation of the food products and high-molecular-weight compounds formed by prolonged heating [45]. This observation can be compared to the results of the reflection coefficient (Figure 10), where the used oil exhibits a slight variation in resonant frequency and a higher response. This proves the ability of the sensor to identify the difference between new and used oil according to their compositional and physical differences.

Figure 12 demonstrates the viscosity of new cooking oil and used cooking oil, which indicates a clear difference in flow behavior. The viscosity of new

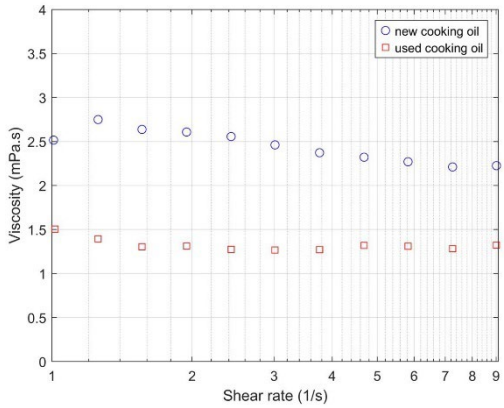

Figure 12: Viscosity as a function of shear rate for new cooking and used cooking oil.

cooking oil (2.2–2.7 mPa·s) is significantly higher than that of used cooking oil (1.3–1.5 mPa·s). At the initial rate, new and used cooking oil show nearly Newtonian behaviour. However, the increasing shear rate of the new oil tends to display a weak shear-thinning pattern. The used cooking oil maintains a more constant profile, indicating behaviour closer to an ideal Newtonian fluid [46]. This decrease in the viscosity after repeated use could be explained by thermal degradation and oxidation during the frying process that breaks down triglycerides to smaller molecules and weakens intermolecular bonding. Thus, leading to a less viscous fluid [47], [48]. This viscosity degradation not only reflects the deterioration of oil, but it is also correlated with the variations of the reflection coefficient, as was observed by the metamaterial-based sensor. Overall, the consistent correlation between the microwave sensing characteristics, the FTIR spectral changes, the reduction in viscosity, and the visual degradation verifies the capability of the proposed metamaterial-based sensor to sensitively and non-destructively differentiate between fresh and deteriorated cooking oils.

4 Conclusions

A highly sensitive metamaterial resonant sensor has been successfully developed and validated for nondestructive food quality monitoring. In the proposed sensor, strong resonance characteristics have been achieved with a high Q-factor of 43.498. The sensor's sensing characteristics are determined based on changes in resonant frequency, reflection coefficient, and FWHM bandwidth. The sensor successfully demonstrated its ability to detect a minimum difference of 0.3% moisture content in cooking powder samples, thus proving its high sensitivity characteristics. For liquid food samples, honey and cooking oil, significant changes in resonant frequency and Q-factors have been observed and correlated based on moisture content, sugar content, viscosity, and molecular structure. The sensor successfully distinguished between new and used cooking oil via a measurable shift of 0.1 GHz frequency and changes in Q-factors, thus proving its ability to detect oil degradation due to thermal oxidation. These results demonstrate the reliability, sensitivity, and applicability of the sensor in real-world applications like food quality analysis, oil degradation analysis, and non-destructive testing in food processing industries. However, the use of an FR-4 substrate with quite high dielectric losses may limit further sensitivity enhancement, and the study was conducted under laboratory conditions with a limited range of samples. Future work will focus on low-loss substrates, improved resonator optimization, and validation across a broader range of food products to enable real-time industrial implementation.

Acknowledgments

Special thanks to Muhammad Izzat Hafizuddin Mohd Shah and Mohd Azman Mohd Sadikin for their assistance with the sample characterizations, and to Muhammad Amiruddin Hassan Al Ashari for his help with the microwave network measurement of the metamaterial-based sensor. Their invaluable support is gratefully acknowledged, with thanks to the UTHM Laboratory Management Office - Pagoh Branch Campus for facilitating these efforts. Communication of this research is made possible through monetary assistance by Universiti Tun Hussein Onn Malaysia and the UTHM Publisher's Office via Publication Fund E15216.

Author Contributions

Fahmiruddin Esa: Conceptualization, Methodology, Investigation, Data Curation, Formal Analysis, Writing – Original Draft Preparation, Writing – Review & Editing, Supervision, Project Administration, Funding Acquisition. Nurdiana Anis Ibrahim: Investigation,

Data Curation. Huda A. Majid: Methodology, Software, Formal Analysis, Writing – Review & Editing. Sim Man Seng and You Kok Yeow: Writing – Review & Editing. All authors have read and agreed to the published version of the manuscript.

Conflicts of Interest

Authors declare that there is no conflict of interest regarding the publication of the paper.

Declaration of generative AI and AI-assisted technologies in the writing process

The authors utilized the ChatGPT tool to enhance the language and readability of the manuscript.

References

[1] M. V. Zambrano, B. Dutta, D. G. Mercer, H. L. MacLean, and M. F. Touchie, "Assessment of moisture content measurement methods of dried food products in small-scale operations in developing countries: A review," *Trends in Food Science & Technology*, vol. 88, pp. 484–496, Jun. 2019. doi: 10.1016/j.tifs. 2019.04.006

[2] H. Niu, M. Zhang, D. Shen, A. S. Mujumdar, and Y. Ma, "Sensing materials for fresh food quality deterioration measurement: a review of research progress and application in supply chain," *Critical Reviews in Food Science and Nutrition*, pp. 1–19, Apr. 2023. doi: 10. 1080/10408398. 2023.2195939

[3] R. T. Blakey and A. M. Morales-Partera, "Microwave dielectric spectroscopy – A versatile methodology for online, non-destructive food analysis, monitoring and process control," *Engineering in Agriculture, Environment and Food*, vol. 9, no. 3, pp. 264–273, Jul. 2016.

[4] R. Raju, G. E. Bridges, and S. Bhadra, "Wireless passive sensors for food quality monitoring: Improving the safety of food products," *IEEE Antennas and Propagation Magazine*, vol. 62, no. 5, pp. 76–89, Oct. 2020.

[5] N. Miura, S. Yagihara, and S. Mashimo, "Microwave dielectric properties of solid and liquid foods investigated by time-domain reflectometry," *Journal of Food Science*, vol. 68, no. 4, pp. 1396–1403, May 2003, doi: 10.1111/j. 1365-2621.2003.tb09656.x

[6] E. Iaccheri, A. Berardinelli, G. Maggio, T. G. Toschi, and L. Ragni, "Affordable time-domain reflectometry system for rapid food analysis," *IEEE Transactions on Instrumentation and Measurement*, vol. 70, pp. 1–7, 2021, doi: 10.1109/TIM.2021.3069050

[7] H. He et al., "A review of time domain reflectometry (TDR) applications in porous media," *Advances in Agronomy*, pp. 83–155, 2021, doi: 10.1016/bs.agron.2021.02.003

[8] D. Prakash and N. Gupta, "Applications of metamaterial sensors: A review," *International Journal of Microwave and Wireless Technologies*, vol. 14, no. 1, pp. 19–33, Feb. 2021, doi: 10.1017/ s1759078721000039

[9] N. Kazemi, M. Abdolrazzaghi, P. Musilek, and E. Baladi, "A planar compact absorber for microwave sensing based on transmission-line metamaterials," *IEEE Sensors Journal*, pp. 1–1, Jan. 2024.

[10] R. Srivastava and S. N. Kale, "Metamaterial inspired resonators as microwave sensors: A review," *Engineering Science & Technology*, pp. 28–47, Aug. 2023, doi: 10.37256/est.5120242960

[11] M. S. Sim et al., "Microwave sensors loaded with metamaterial-inspired resonators for dielectric material characterization: A review," *Sensors and Actuators A: Physical*, vol. 372, p. 115322, Apr. 2024, doi: 10.1016/j.sna.2024.115 322

[12] Z. Meng, Z. Wu, and J. Gray, "Microwave sensor technologies for food evaluation and analysis: Methods, challenges and solutions," *Transactions of the Institute of Measurement and Control*, vol. 40, no. 12, pp. 3433–3448, Sep. 2017, doi: 10.1177/ 0142331217721968

[13] Y. I. Abdulkarim et al., "Highly sensitive metamaterial-based microwave sensor for the application of milk and dairy products," *Applied Optics*, vol. 61, no. 8, pp. 1972–1972, Feb. 2022, doi: 10.1364/AO.451900

[14] K. Karthikeyan, P. S. Praveen Anandh, M. Ramesh, and V. Saran, "Design and parameter optimization of microwave sensor for fat content detection in milk," *AIP Conference Proceedings*, vol. 3232, pp. 030002–030002, Jan. 2024, doi: 10.1063/5.0236788.

[15] K. Brinker, M. Dvorsky, M. T. Al Qaseer, and R. Zoughi, "Review of advances in microwave and millimetre-wave NDT&E: principles and

applications," *Philosophical Transactions of the Royal Society A: Mathematical, Physical and Engineering Sciences*, vol. 378, no. 2182, p. 20190585, Sep. 2020, doi: 10.1098/rsta.2019. 0585

[16] M. S. Sim, K. Y. You, F. Esa, and Y. L. Chan, "Nanostructured Electromagnetic Metamaterials for Sensing Applications," *Advances in Chemical and Materials Engineering*, pp. 141–164, 2021, doi: 10.4018/978-1-7998-5563-7.ch009.

[17] S. Shamim, A. S. M. Mohsin, M. M. Rahman, and M. Belal, "Recent advances in the metamaterial and metasurface-based biosensor in the gigahertz, terahertz, and optical frequency domains," *Heliyon*, vol. 10, no. 13, pp. e33272–e33272, Jun. 2024. doi: 10.1016 /j.heliyon.2024. e33272

[18] N. Meyne, C. Cammin, and A. F. Jacob, "Accuracy enhancement of a split-ring resonator liquid sensor using dielectric resonator coupling," *in 2014 20th International Conference on Microwaves, Radar and Wireless Communications (MIKON), Gdansk, Poland: IEEE*, Jun. 2014, pp. 1–4. doi: 10.1109/MIKON. 2014.6899869.

[19] M. H. Baharuddin, M. F. Jamlos, M. Jusoh, M. R. Kamarudin, M. F. Jamlos, and M. F. A. Malek, "A review of characterization techniques for material's properties measurement using microwave resonant sensor," *Journal of Telecommunication, Electronic and Computer Engineering*, vol. 10, no. 1-9, pp. 57–61, 2018.

[20] K. Y. You and S. K. Goudos, "Materials characterization using microwave waveguide system," *in Microwave Systems and Applications*, pp. 341–358, 2017, doi: 10.5772/ 66230

[21] T. Dahms, D. B. Hayman, B. Mohamadzade, and S. L. Smith, "Measurement of dielectric properties of thin materials for radomes using waveguide cavities," *Telecom*, vol. 5, no. 3, pp. 706–722, Aug. 2024, doi: 10.3390/telecom 5030036.

[22] S. Harnsoongnoen, "Microwave sensors based on coplanar waveguide loaded with split ring resonators: A review," *Applied Science and Engineering Progress*, vol. 12, no. 4, pp. 224–234, 2019. doi: 10.14416/j.ijast. 2018.11.006

[23] Md. Rashedul Islam et. al., "Metamaterial sensor based on reflected mirror rectangular split ring resonator for the application of microwave sensing," *Measurement*, vol. 198, p. 111416, Jul. 2022. doi: 10.1016/j. measurement.2022.111416

[24] Y. Li et. al., "Dielectric properties of chili powder in the development of radio frequency and microwave pasteurisation," *International Journal of Food Properties*, vol. 20, no. sup3, pp. S3373–S3384, Dec. 2017.

[25] S. Qi et al., "Dielectric properties of edible fungi powder related to radio-frequency and microwave drying," *Food production, processing and nutrition*, vol. 3, no. 1, Jun. 2021.

[26] L. C. Costa, S. S. Teixeira, and F. Henry, "Measuring microwave dielectric properties of materials: Theory and applications," *Materials Research Bulletin*, vol. 179, Art. no. 112976, 2024, doi: 10.1016/j.materresbull. 2024.112976.

[27] A. Alimenti, K. Torokhtii, P. Vidal García, N. Pompeo, and E. Silva, "Design and test of a new dielectric-loaded resonator for the accurate characterization of conductive and dielectric materials," *Sensors*, vol. 23, no. 1, Art. no. 518, 2023, doi: 10.3390/s23010518.

[28] Z. Li, Z. Meng, A. Haigh, P. Wang, and A. Gibson, "Characterisation of water in honey using a microwave cylindrical cavity resonator sensor," *Journal of Food Engineering*, vol. 292, pp. 110373–110373, Mar. 2021. doi: 10.1016/j. jfoodeng.2020.110373

[29] Q. Jin, Z. Meng, Z. Chen, and Z. Li, "Review of scientific instruments: Evaluation of adulteration in honey using a microwave planar resonator sensor," *Review of Scientific Instruments*, vol. 94, no. 10, Oct. 2023, doi: 10.1063/5.0166005

[30] I. Singh and S. Singh, "Honey moisture reduction and its quality," *Journal of Food Science and Technology*, vol. 55, no. 10, pp. 3861–3871, 2018, doi: 10.1007/s13197-018-3341-5

[31] W. Guo, X. Zhu, Y. Liu, and H. Zhuang, "Sugar and water contents of honey with dielectric property sensing," *Journal of Food Engineering*, vol. 97, no. 2, pp. 275–281, Mar. 2010, doi : 10.1016/j.jfoodeng.2009.10.024

[32] K. Polatidou, C. Nouska, C. Tananaki, C. G. Biliaderis, and A. Lazaridou, " Physicochemical and rheological characteristics of monofloral honeys—kinetics of creaming–crystallization,"

Foods, vol. 14, no. 10, pp. 1835 May 2025, doi:10.3390/foods14101835

[33] T. Castillo Martínez, C. García Osorio, J. G. García Muñiz, J. Aguilar Ávila, & R. Ramírez Valverde, "Sugars and °Brix in honey from *Apis mellifera, Melipona beecheii,* and commercial honey from a local market in Mexico," *Veterinaria México OA,* vol. 9, Sep. 2022, doi:10.22201/fmvz.24486760e.2022.950.

[34] M. Sahlan, S. Karwita, M. Gozan, H. Hermansyah, M. Yohda, Y. J. Yoo, & D. K. Pratami, "Identification and classification of honey's authenticity by attenuated total reflectance Fourier-transform infrared spectroscopy and chemometric method," *Veterinary World*, vol. 12, no. 8, pp. 1304–1310, Aug. 2019, doi:10.14202/vetworld. 2019.1304-1310.

[35] N. D. Rodrigues, S. C. Palomares, and E.-R. E. Mojica, "Multivariate analysis of the ATR-FTIR of honey samples," *Journal of Undergraduate Chemistry Research,* vol. 24, no. 1, pp. 33–37, Feb. 2025.

[36] O. Escuredo, I. Dobre, M. Fernández-González, and M. C. Seijo, "Contribution of botanical origin and sugar composition of honeys on the crystallization phenomenon," *Food Chemistry*, vol. 149, pp. 84–90, Apr. 2014. doi : 10.1016/ j.foodchem.2013.10.097

[37] M. A. Al-Kafaween, M. Alwahsh, A. B. Mohd Hilmi, and D. H. Abulebdah, "Physicochemical characteristics and bioactive compounds of different types of honey and their biological and therapeutic properties: A comprehensive review," *Antibiotics*, vol. 12, no. 2, Art. 337, 2023, doi: 10.3390/antibiotics12020337

[38] P. M. da Silva, C. Gauche, L. V. Gonzaga, A. C. O. Costa, and R. Fett, "Honey: Chemical composition, stability and authenticity," *Food Chemistry*, vol. 196, pp. 309–323, Apr. 2016, doi: 10.1016/j.foodchem.2015.09.051.

[39] S. Yahya, F. H. Razali, and F. W. Harun, "Physicochemical properties of refined palm cooking oil and used palm cooking oil," *Materials Today: Proceedings*, vol. 19, pp. 1166–1172, 2019, doi: 10.1016/j.matpr.2019. 11.010

[40] P. S. Dewi and M. Ulfah, "Quality test of palm cooking oil used repeatedly based on free fatty acid content, moisture content, peroxide number," *Journal of Science and Technology Research for Pharmacy*, vol. 1, no. 1, pp. 34–41, Mar. 2021. doi: 10.15294/jstrp. v1i1.44461

[41] A. A. A. Wahab, S. H. Chang, and A. M. Som, "Characterization of waste cooking oil as a potential green solvent for liquid-liquid extraction," *Proceedings of the International Conference on Advances in Civil and Environmental Engineering (ACEE 2015)*, Penang, Malaysia, 2015, doi: 10. 1371/journal. pone.0232997

[42] S. M. Alshuiael and M. Al-Ghouti, "Multivariate analysis for FTIR in understanding treatment of used cooking oil using activated carbon prepared from olive stone," *PLoS ONE*, vol. 15, no. 5, May 2020, doi: 10.1371/journal.pone.0232997

[43] M. M. Hassanein, S. M. El-Shami, and M. Hassan El-Mallah, "Changes occurring in vegetable oils composition due to microwave heating," *Grasas aceites*, vol. 54, no. 4, pp. 343–349, Dec. 2003, doi : 10.3989/ gya.2003.v54.i4. 219

[44] X. Chen and S. Sun, "Color reversion of refined vegetable oils: A review," *Molecules*, vol. 28, no. 13, Art. 5177, 2023, doi : 10.3390/molecules 28135177

[45] Q. Li et al., " Indication of the color change on the oxidation properties of fragrant rapeseed oil during shelf storage," *Food Chemistry: X*, vol. 20, art. no. 100908, 2023, doi: 10.1016/j.fochx. 2023.100908.

[46] S. N. Sahasrabudhe, J. A. Staton, and B. E. Farkas, "Effect of frying oil degradation on surface tension and wettability," *LWT*, vol. 99, pp. 519–524, Jan. 2019. doi: 10.1016/j.lwt. 2018.10.026

[47] L. Cui, J. Chen, J. Zhai, L. Peng, and D. Hayes, " Oil penetration of batter-breaded fish nuggets during deep-fat frying: effect of frying oils," *Foods*, vol. 11, no. 21, pp. 3369, Oct. 2022. doi : 10.3390/foods11213369

[48] B. Wiege, E. Fehling, B. Matthäus, and M. Schmidt, " Changes in physical and chemical properties of thermally and oxidatively degraded sunflower oil and palm fat," *Foods*, vol. 9, no. 9, pp. 1273, Sep. 2020. doi : 10.3390/foods 9091273